doi:10.1016/j.jmb.2008.12.075 J. Mol. Biol. (2009) 386, 1167–1178

JMB

Available online at www.sciencedirect.com

ScienceDirect

ELSEVIER

Structural Rearrangements Linked to Global Folding Pathways of the *Azoarcus* Group I Ribozyme

Seema Chauhan[1], Reza Behrouzi[2], Prashanth Rangan[2] and Sarah A. Woodson[2]*

[1]*Department of Chemistry, Johns Hopkins University, Baltimore, MD 21218-2685, USA*

[2]*T.C. Jenkins Department of Biophysics, Johns Hopkins University, Baltimore, MD 21218-2685, USA*

Received 7 November 2008; received in revised form 19 December 2008; accepted 29 December 2008
Available online 6 January 2009

Stable RNAs must fold into specific three-dimensional structures to be biologically active, yet many RNAs form metastable structures that compete with the native state. Our previous time-resolved footprinting experiments showed that *Azoarcus* group I ribozyme forms its tertiary structure rapidly ($\tau < 30$ ms) without becoming significantly trapped in kinetic intermediates. Here, we use stopped-flow fluorescence spectroscopy to probe the global folding kinetics of a ribozyme containing 2-aminopurine in the loop of P9. The modified ribozyme was catalytically active and exhibited two equilibrium folding transitions centered at 0.3 and 1.6 mM Mg^{2+}, consistent with previous results. Stopped-flow fluorescence revealed four kinetic folding transitions with observed rate constants of 100, 34, 1, and 0.1 s^{-1} at 37 °C. From comparison with time-resolved Fe(II)-ethylenediaminetetraacetic acid footprinting of the modified ribozyme under the same conditions, these folding transitions were assigned to formation of the I_C intermediate, tertiary folding and docking of the nicked P9 tetraloop, reorganization of the P3 pseudoknot, and refolding of nonnative conformers, respectively. The footprinting results show that 50–60% of the modified ribozyme folds in less than 30 ms, while the rest of the RNA population undergoes slow structural rearrangements that control the global folding rate. The results show how small perturbations to the structure of the RNA, such as a nick in P9, populate kinetic folding intermediates that are not observed in the natural ribozyme.

Keywords: RNA folding; ribozyme; stopped-flow fluorescence; time-resolved footprinting; 2-aminopurine

Edited by J. Doudna

Introduction

The formation of tertiary structure allows RNAs to function efficiently as catalysts, aptamers, and switches.[1–3] While some RNAs fold in 10–100 ms, other RNA sequences become kinetically trapped in alternative conformations that persist for 10–100 s or longer.[4–6] Theoretical models and experimental results suggest that the partitioning of the RNA population between folding pathways that lead to the native structure or to an alternative metastable structure occurs early in the folding pathway.[7] Therefore, it is important to understand which interactions determine the folding kinetics of the RNA and the uniqueness of the folding pathway.

The group I ribozyme from pre-$tRNA^{ile}$ of the bacterium *Azoarcus* sp. BH72 forms a stable structure[8] and folds rapidly at 37–50 °C without significantly becoming trapped in metastable kinetic intermediates.[9,10] The equilibrium folding pathway in Mg^{2+} involves at least two macroscopic transitions (Scheme 1). In the $U \rightarrow I_C$ transition, which occurs around 0.2–0.3 mM $MgCl_2$, the core helices are assembled and the RNA collapses into native-like intermediates (I_C) with similar dimensions as the native RNA.[11] Small-angle X-ray scattering (SAXS) studies showed that tertiary interactions between helices stabilize I_C, although solvent can still penetrate the interior of the ribozyme.[12] In the

*Corresponding author. E-mail address: swoodson@jhu.edu.

Present addresses: S. Chauhan, Xbiotech USA Inc., Austin, TX-78749, USA; P. Rangan, Skirball Institute of Biomolecular Medicine, New York University Medical School, 540 First Avenue, New York, NY 10016, USA.

Abbreviations used: SAXS, small-angle X-ray scattering; 2-AP, 2-aminopurine; EDTA, ethylenediaminetetraacetic acid.

0022-2836/$ - see front matter

$I_C \rightarrow N$ transition, which occurs in 2–3 mM $MgCl_2$, the native tertiary interactions between helices are fully established and the RNA becomes catalytically active.

$$U \leftrightarrow I_C \leftrightarrow N \qquad \text{Scheme 1}$$

Using time-resolved hydroxyl radical footprinting, which reveals the backbone accessibility of individual riboses, we found that the wild-type *Azoarcus* ribozyme folds to its native tertiary structure (N) in 5–20 ms at 37 °C.[10] To study the global folding kinetics of the *Azoarcus* ribozyme, we tagged a tetraloop in the ribozyme with the fluorescent adenine analog 2-aminopurine (2-AP).[13] 2-AP forms an isosteric Watson–Crick-type base pair with uracil and, thus, causes minimal perturbation to RNA secondary structure. It has been widely used to study conformational changes in nucleic acids[14] because the quantum yield of the fluorescence is sensitive to the local $\pi \rightarrow \pi*$ stacking interactions with neighboring nucleobases.[13,15]

Here, we find that the change in the fluorescence of a 2-AP-tagged ribozyme is consistent with the Mg^{2+}-dependent equilibrium folding pathway previously deduced from other biochemical and biophysical methods.[9,11,12] Analysis of the folding kinetics with a stopped-flow spectrofluorometer showed that the intermediate forms with $\tau \leq 10$ ms and that the tertiary folding occurs with $\tau \leq 30$ ms, consistent with the results of time-resolved hydroxyl radical footprinting experiments. However, the folding kinetics of the tagged ribozyme reveals at least two additional steps in the folding process. We attribute one of these additional steps to refolding of the P3 pseudoknot in a subpopulation of nonnative intermediates. A second slow transition is assigned to reorganization of the ribozyme core after the P3 pseudoknot is formed.

Results

Fluorophore-tagged *Azoarcus* ribozyme

The native state of the *Azoarcus* ribozyme is stabilized by docking of the GAAA tetraloop in paired region P9 into a receptor in P5/P5a.[8,16,17] We previously found that this interaction also stabilizes the compact folding intermediates (I_C) of the ribozyme.[12] Thus, tetraloop-receptor docking is expected to report the folded state of the ribozyme. The third base in the GAAA tetraloop (A191) was replaced by 2-AP (Fig. 1a) to monitor the folding transitions in the ribozyme. Tetraloop docking involves a network of hydrogen bonding and additional base-stacking interactions between purines in the P9 loop and bases in the receptor (Fig. 1b).[19] Therefore, the fluorescence emission of 2-AP191 is expected to be perturbed in the native ribozyme, relative to the undocked tetraloop.

The desired 2-AP substitution at A191 was introduced by annealing a synthetic 14-nt RNA (OP9G) containing the 3′ end of the ribozyme (2-AP or A191 to G205) with a 187-nt T7 transcript (IΔP9) that provides the rest of the ribozyme (G4 to A190) (Fig. 1a). This strategy was successfully used for crystallization of the *Azoarcus* splicing complex[17] and modification of a group II ribozyme.[20] Cleavage of the 5′ splice site and hydroxyl radical footprinting of the folded RNA demonstrated that the 2-AP-labeled ribozyme complex was active and formed the expected tertiary contacts (Fig. S1). The results also confirmed that the IΔP9 RNA does not fold correctly without the OP9G oligonucleotide.

To determine the best conditions for folding experiments, we measured the binding affinity of

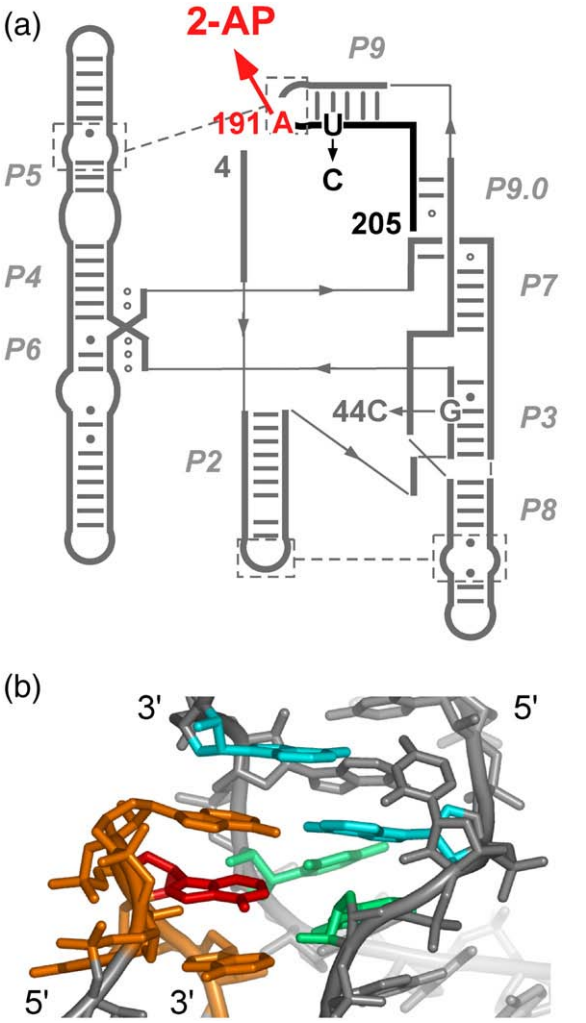

Fig. 1. (L-3) *Azoarcus* ribozyme labeled with 2-AP. (a) The fluorescent ribozyme was reconstituted by annealing (L-3) IΔP9 (gray) with OP9G oligomer (black) in 10 mM Tris buffer (pH7.5) at 65 °C for 2 min. A191 (red) was replaced by 2-AP. The U194C mutation in P9 (black) and the G44C mutation in P3 are also shown. (b) Structure of GAAA tetraloop (orange/red) and 11 nt receptor complex (1hr2),[18] rendered with PyMOL (Delano Scientific). The adenosine replaced by 2-AP in the labeled ribozyme is shown in red. Interacting bases in the receptor are shown in green and cyan.

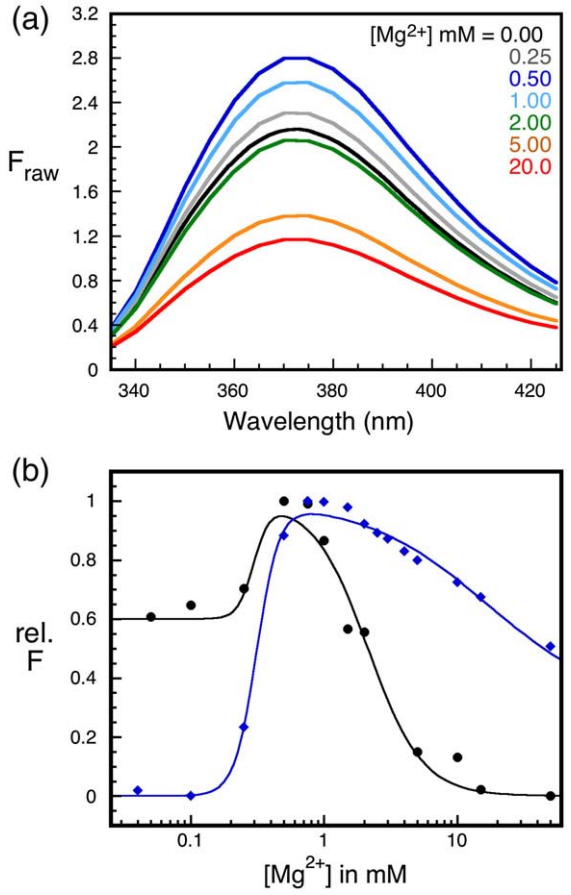

Fig. 2. Folding equilibrium of the *Azoarcus* ribozyme by steady-state fluorescence. (a) Emission spectra of the fluorescent wild-type ribozyme at 37 °C, with excitation at 310 nm. (b) Relative fluorescence intensity (F) at 370 nm in wild-type (black) and P3 mutant (blue) ribozyme *versus* Mg^{2+} concentration. Data were fit to a three-state model as described in Materials and Methods. Parameters for statistical weights for wild type: $C_I = 0.29$, $m = 5.0$; $C_N = 0.53$, $n = 7.1$; P3: $C_I = 0.31$, $m = 5.2$; $C_N = 0.58$, $n = 6.2$. Uncertainty in fitted parameters is ±20%. As shown in Fig. 3, the corresponding transition midpoints for the wild type are as follows: $C_{m,I} = 0.27 \pm 0.04$ mM, $n_{H,I} = 5 \pm 2$; $C_{m,N} = 1.6 \pm 0.2$ mM, $n_{H,N} = 1.7 \pm 0.3$; P3: $C_{m,I} = 0.31 \pm 0.01$ mM, $n_{H,I} = 5 \pm 1$; $C_{m,N} = 15 \pm 2$ mM, $n_{H,I} = 1.0 \pm 0.2$.

the fluorescent oligonucleotide to the IΔP9 transcript by a gel-mobility shift assay (Fig. S2a). In the unfolded state (10 mM Tris–HCl buffer), the dissociation constant (K_d) of OP9G was 1.7± 0.8 μM. The addition of 0.5 mM Mg^{2+} or 50 mM Na^+ to the annealing buffer significantly decreased the K_d to 89±6 and 490±30 nM, respectively (Fig. S2b). Consequently, RNA (≥2 μM) was initially annealed in 0.5 mM Mg^{2+} for kinetic folding experiments to ensure that all of the fluorescent oligomer was bound. However, as folding intermediates (I_C) of the *Azoarcus* ribozyme form in submillimolar magnesium,[9,11] our kinetic folding experiments start from a mixture of I_C and U, which may contribute to the heterogeneity of the observed time constants as described below.

Equilibrium folding monitored by steady-state fluorescence

To determine if the change in fluorescence intensity of 2-AP reports the known folding transitions of the *Azoarcus* ribozyme, we measured the steady-state fluorescence of the IΔP9·OP9 complex over a range of Mg^{2+} concentrations (Fig. 2a). Two transitions were observed when Mg^{2+} was added to the IΔP9·OP9 complex. In the first phase, the 2-AP fluorescence signal increased with Mg^{2+} up to 0.5 mM. This was followed by a cooperative decrease in fluorescence intensity upon further addition of Mg^{2+} up to 20 mM (Fig. 2b). As expected, the fluorescence intensity of the OP9G oligomer alone changed negligibly under these conditions.

The change in relative 2-AP fluorescence was fit to a three-state cooperative binding model for Mg^{2+}, as described in Materials and Methods (Fig. 2b). The populations of U, I_C, and N states predicted from the fits (Fig. 3a) corresponded to a cooperative

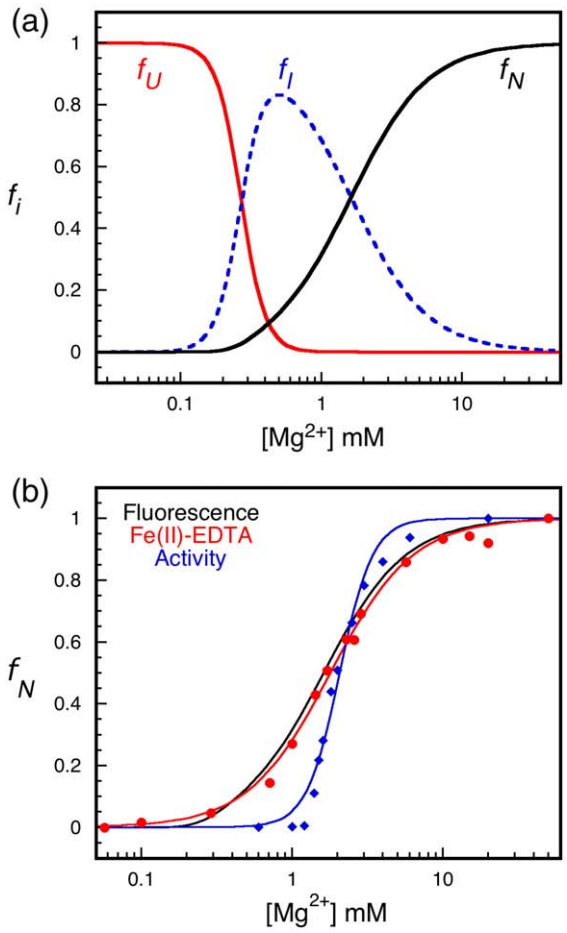

Fig. 3. Comparison of folding monitored by fluorescence and biochemical probes. (a) Fraction of unfolded (U), intermediate (I_C), and native (N) ribozyme predicted by three-state fits to fluorescence intensity as a function of Mg^{2+} concentration as in Fig. 2b. (b) Fraction native RNA (f_N) from fluorescence experiments (black line), hydroxyl radical cleavage (red circles, nucleotides 62–64, from Ref. [10]) and activity at 32 °C (blue diamonds, data from Ref. [12]). Data were fit to the Hill equation (see Table 1).

Table 1. Folding equilibria of the *Azoarcus* ribozyme from different experimental techniques

	U→I_C		I_C→N	
Technique	C_I (mM)	n_H	C_N (mM)	n_H
SAXS[a]	0.34±0.01	2.7±0.01	—	—
RNase T1[b]	0.2–1.1	1.2–12.6	—	—
Fluorescence[c]	0.27±0.04	5±2	1.6±0.2	1.6±0.3
Fe(II)-EDTA[d]	—	—	0.7–1.8	1.2–2.4
Activity[b]	—	—	1.97±0.06	4.5±0.5

[a] Data from Ref. [12] collected at 32 °C.
[b] Data from Ref. [12] collected at 50 °C. Reported are the mean and standard deviation of three independent trials.
[c] Fractions of U, I, and N states at 37 °C were used to obtain the parameters for the U→I and I→N transitions, respectively.
[d] Data from Ref. [10] collected at 50 °C.

loss of unfolded RNA with an apparent midpoint of $C_{m,I}$=0.27±0.04 mM and a Hill coefficient of $n_{H,I}$=5±2 and an increase in native RNA with $C_{m,N}$=1.6±0.2 mM and $n_{H,N}$=1.6±0.3 (Fig. 3a).

These parameters agreed closely with those obtained by other biophysical and biochemical methods (Fig. 3b and Table 1), confirming that the 2-AP fluorescence reports the same folding transitions detected previously.[12] The midpoint of the first folding transition agreed, within experimental error, with midpoints for the decrease in the radius of gyration (R_g) measured by SAXS (0.34 mM) and the protection from ribonuclease T1 digestion (0.2–1.1 mM) (Table 1), which both report the transition from U to I_C. The midpoint of the second fluorescence transition overlapped the I_C→N tertiary folding transition, as monitored by hydroxyl radical cleavage (C_m=0.7–1.8 mM) and the onset of catalytic activity (C_m=2.0 mM) (Fig. 3b). Thus, the change in fluorescence reflects Mg^{2+}-induced folding of the *Azoarcus* ribozyme, and the folding equilibrium is not severely perturbed by the modification.

The increase in 2-AP fluorescence during the U→I_C folding transition may be due to improved hybridization of the OP9G oligonucleotide or to a change in the environment of the 2-AP in the P9 tetraloop in the collapsed state. The decrease in 2-AP fluorescence in the I_C→N step at higher Mg^{2+} is probably due to stacking of 2-AP with bases in the P5/5a receptor. There is precedence for different folding steps having opposite effects on the environment of the fluorophore probe. For example, the fluorescein-labeled catalytic domain of RNase P exhibits a decrease and increase in fluorescence signal during its U→I_{eq} and I_{eq}→N folding transitions, respectively.[21]

Ribozyme core mutation perturbs folding monitored by fluorescence

To verify that the fluorescence of 2-AP191 reports global folding and not just local perturbation of the tetraloop, we repeated the equilibrium folding experiments with a ribozyme containing the mutation G44C in the P3 pseudoknot within the ribozyme core. Disruption of P3 by this base substitution destabilizes both the compact intermediate (I_C) and the native state (N) of the *Azoarcus* ribozyme.[12]

The same changes in fluorescence intensity were observed, but much more Mg^{2+} was needed to fold the P3 mutant RNA (Fig. 2b). Although the midpoint of the first U→I_C transition ($C_{m,I}$=0.32±0.01 mM) was only slightly higher for the P3 mutant than for the wild-type ribozyme, the midpoint of the second I_C→N transition was 10 times higher ($C_{m,N}$=17±2 mM) than for the wild-type (Fig. 2b). Moreover, the P3 2-AP-tagged RNA did not fold completely, even in 50 mM $MgCl_2$. This observation is consistent with the larger R_g and reduced catalytic activity (40%) of the P3 ribozyme observed previously.[12] Thus, the change in fluorescence reflects the global structure of the RNA and not just changes in the local environment of the probe.

Folding kinetics of the *Azoarcus* ribozyme by time-resolved fluorescence

The *Azoarcus* ribozyme forms its native 3D structure in τ ~ 10–30 ms, with 10–20% of the wild-type population becoming kinetically trapped in misfolded intermediates at 37 °C.[10] As the U→I_C and I_C→N transitions produce opposite changes in 2-AP fluorescence, we used stopped-flow fluorescence spectroscopy to capture the kinetics of both steps. The folding kinetics of the *Azoarcus* ribozyme was monitored by mixing the annealed IΔP9·OP9G complex with $MgCl_2$-containing buffer in a stopped-flow spectrofluorometer (see Materials and Methods). To ensure that the folding rate was not limited by binding of OP9G, we used a large excess of (L-3) IΔP9 RNA (typically 10 μM). Above 4 μM RNA, the observed folding rates are independent of RNA concentration (Fig. S3).

Under native conditions (15 mM Mg^{2+}), we observed at least four kinetic phases within the first 10 s of each trajectory. A fast increase in fluorescence ($k_{obs,1}$=106 s^{-1}) was followed by two slower phases of decreasing fluorescence ($k_{obs,2}$=34 s^{-1}; $k_{obs,3}$=1 s^{-1}) (Fig. 4a, inset). When the ribozyme was allowed to fold for a longer period of time (10 s), an additional slow decrease in fluorescence appeared, with an apparent rate constant, $k_{obs,4}$=0.1–0.3 s^{-1} (Fig. 4a). A comparison of three- and four-phase fits to the entire trajectory confirmed the presence of four qualitatively distinct kinetic transitions between 10^{-3} and 10 s (Fig. S4). As we describe below, this complexity arises from the two equilibrium folding transitions (U→I_C→N) and from partitioning of the tagged ribozyme complex among folding pathways that include misfolded intermediates.

The rapid increase in fluorescence (≥100 s^{-1}) correlates with the rate of compaction of the *Azoarcus* ribozyme measured by stopped-flow SAXS (J. H. Roh, personal communication) and was assigned to the U→I_C step. Because I_C is already partially populated at the start of the experiment and this step occurs very near the dead time of our instrument, 100 s^{-1} represents the lower limit of the U→I_C rate constant. The apparent rate constant of the second phase (34 s^{-1}) is close to the lower limits of the folding rate observed by time-resolved hydroxyl

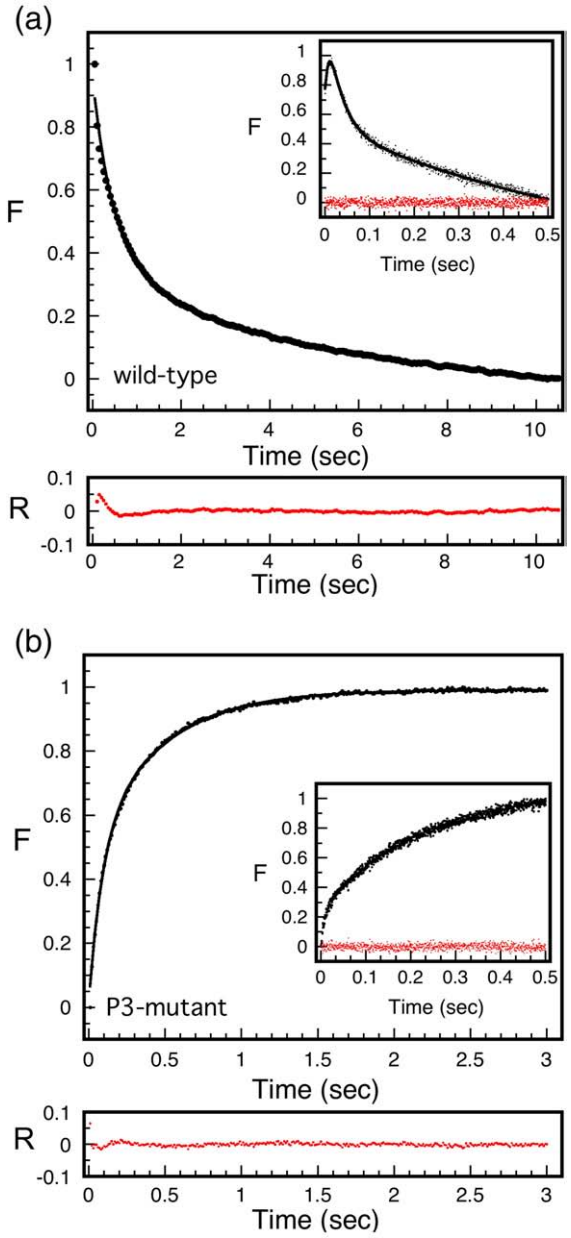

Fig. 4. Folding kinetics by stopped-flow fluorescence. The relative change in 2-AP fluorescence in 15 mM $MgCl_2$ at 37 °C for (a) wild-type and (b) mutant P3 (G44C) ribozymes (see Materials and Methods). Observed rate constants: wild-type: $k_3 = 2.2 \pm 0.1$ s^{-1}, $A_3 = 0.6 \pm 0.2$; $k_4 = 0.23 \pm 0.01$ s^{-1}, $A_4 = 0.4 \pm 0.2$; P3 mutant: $k_3 = 11.8 \pm 0.3$ s^{-1}, $A_3 = 0.49 \pm 0.01$; $k_4 = 2.24 \pm 0.03$ s^{-1}, $A_4 = 0.51 \pm 0.01$. Residuals of the curve fit are shown in red. Insets: Change in fluorescence over 500 ms. Wild-type: $k_1 = 106 \pm 14$ s^{-1}, $A_1 = 0.8 \pm 0.1$; $k_2 = 34 \pm 1$ s^{-1}, $A_2 = 0.4 \pm 0.2$; $k_3 = 1 \pm 0.5$ s^{-1}, $A_3 = 0.6 \pm 0.1$; P3 mutant: $k_1 = 115 \pm 4$ s^{-1}, $k_2 = 5 \pm 1$ s^{-1}, $k_3 = 0.010 \pm 0.007$ s^{-1}. Reported are the mean and standard deviation of three independent trials.

radical cleavage (30–100 s^{-1})[10]. This, and the correlation between a decrease in fluorescence and population of the native state in the equilibrium Mg^{2+} titrations (Fig. 3), led us to assign the second kinetic phase to a tertiary folding transition ($I_C \rightarrow N$) of the *Azoarcus* ribozyme.

The third phase (~1 s^{-1}), in which the fluorescence continues to decrease, represents either an additional structural rearrangement that was not detected in previous footprinting experiments or molecules in the RNA population that fold via a separate (parallel) transition-state ensemble. Finally, the slowest decrease in fluorescence ($k_{obs,4} = 0.12$ s^{-1}) most likely corresponds to a reorganization of the ribozyme tertiary structure linked to the conformation of the active site, as it was only detected when the labeled OP9G oligonucleotide included the ribozyme's penultimate G205 (Fig. 4a). When the 0.5- and 10-s data were appropriately scaled and concatenated, the slowest kinetic phase accounted for ~45% of the total decrease in fluorescence.

Thus, the sensitivity of the fluorescence probe reveals additional kinetic folding transitions in the *Azoarcus* ribozyme that are not visible in the equilibrium folding pathway and the enormous range of the folding dynamics (≤10 ms to 10 s). Below, we use time-resolved footprinting to show that the slow steps arise from misfolded intermediates that become populated when P9 is nicked and modified, explaining why these slow transitions were not detected in previous experiments with the single-transcript ribozyme.[10]

P3 mutant delays rapid folding kinetics of the *Azoarcus* ribozyme

To determine if the folding kinetics of the *Azoarcus* ribozyme is sensitive to the stability of the tertiary structure, we also carried out stopped-flow fluorescence experiments with the 2-AP-tagged P3 mutant (G44C). Unlike the wild-type RNA, the P3 mutant ribozyme showed three kinetic phases: a fast increase in fluorescence intensity (115 s^{-1}) followed by a slower increase in fluorescence (5 s^{-1}) (Fig. 4b) and finally an extremely slow decrease in fluorescence (~0.01 s^{-1}) that was only observed at high Mg^{2+}. Our previous SAXS studies[12] and the steady-state fluorescence measurements showed that the P3 mutant undergoes a collapse transition but produces an intermediate that is less compact than the wild-type intermediates. The nonnative conformation of the intermediates and the marginal stability of the native structure could explain why the P3 mutant takes much longer to fold (0.01 s^{-1}) than the wild-type RNA (30 s^{-1}). Thus, destabilization of the core P3 pseudoknot not only alters the average conformation of the I and N states but also significantly delays formation of the tertiary structure, reflecting a tight correlation between the thermodynamic stability of the RNA tertiary structure and the speed and accuracy of the RNA folding process.

Temperature-dependent folding kinetics of the *Azoarcus* ribozyme

The activation energy for the tertiary folding of the wild-type 2-AP-tagged ribozyme was determined from the temperature dependence of its folding

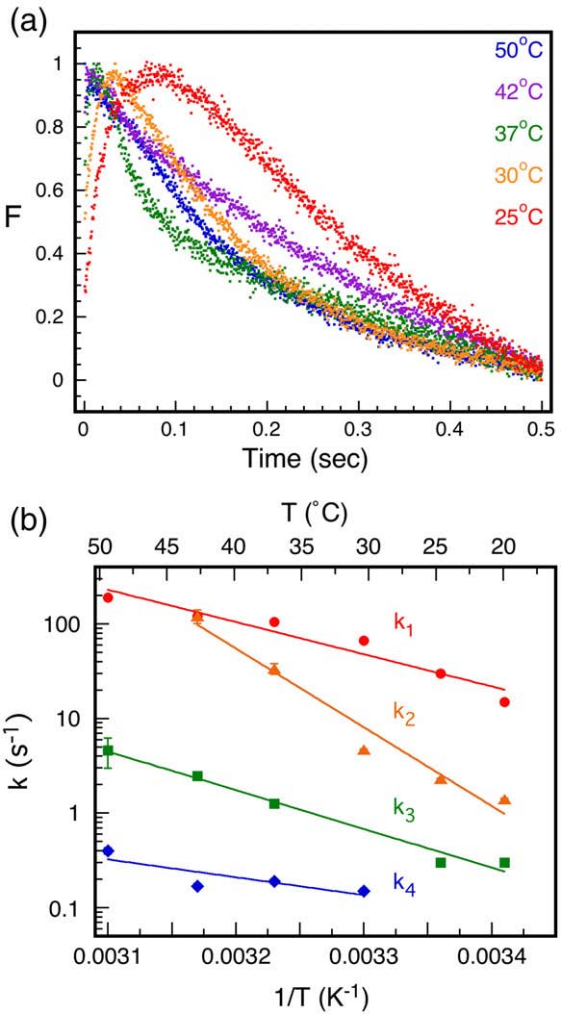

Fig. 5. Temperature dependence of folding kinetics. (a) Folding kinetics at various temperatures (20–50 °C) collected over a 500-ms time window. Trajectories were normalized to the minimum and maximum intensity within this time interval. (b) Arrhenius plot for folding of the *Azoarcus* ribozyme. The observed rate constants were averaged over three independent trials. Symbols: red circles, k_1, $E_{a,1}$=16 kcal/mol; orange triangles, k_2, $E_{a,2}$=35 kcal/mol; green squares k_3, $E_{a,3}$=19 kcal/mol; blue diamonds, k_4, $E_{a,4}$=9 kcal/mol.

kinetics. The annealed (L-3) IΔP9RNA·OP9G complex was pre-equilibrated at each temperature for 10 min, before the folding reaction was started by addition of 15 mM $MgCl_2$ (Fig. 5a). Individual traces were collected for 0.5 and 10 s in order to cover the full time window of the folding reactions, and the average rate constants were plotted as a function of temperature, from 20 to 50 °C (Fig. 5b). Because the transitions were well separated in time, it was possible to assign each kinetic phase of the fluorescence signal to a separate relaxation step over most of the temperature range.

The activation energies for each phase were $E_{a,1}$=16 kcal/mol, $E_{a,2}$=35 kcal/mol, $E_{a,3}$=19 kcal/mol, and $E_{a,4}$=9 kcal/mol (Fig. 5b). These values are within the range reported for other RNA folding reactions, such as folding of the full-length *Tetrahymena* intron (21 kcal/mol),[22–24] formation of mRNA pseudoknot (34 kcal/mol),[25] and folding of catalytic domain of RNase P (32–36 kcal/mol).[21] Thus, most steps are associated with a significant transition-state enthalpy, consistent with changes in base-stacking interactions and hydrogen bonds. The smallest activation energy (9 kcal/mol) for the slowest kinetic phase points to an entropic barrier for the conformational rearrangement associated with the penultimate G205. An entropic barrier was previously reported for the docking of a pyrene-labeled substrate in the *Tetrahymena* ribozyme and may be a signature for structural rearrangements within the active site of group I ribozymes.[26]

Magnesium-dependent folding kinetics of the *Azoarcus* ribozyme

To further elucidate the origin of the complex folding dynamics of the *Azoarcus* ribozyme, we determined the magnesium dependence of the folding kinetics as described above (Fig. 6). If the ribozyme follows a simple two-state folding reaction, then the folding and unfolding rate constants should depend exponentially on Mg^{2+} concentration, producing a "chevron" profile as observed in the dependence of protein folding kinetics on denaturant.[27] Since the folding mechanism of the *Azoarcus* ribozyme is more complex, it is expected to deviate from this simple scenario.[28] Nonetheless, we found that the observed rate constant for each phase increased with Mg^{2+} concentration above the midpoint of the transition (C_m), as expected if the folding rate depends on the stability of the folded RNA (Fig. 6).

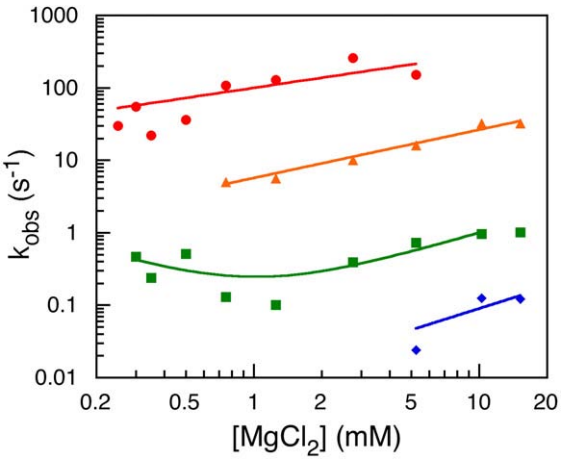

Fig. 6. Magnesium dependence of folding kinetics. Observed folding rate constants (37 °C) in 0.38 to 15 mM $MgCl_2$ (final). Traces were averaged over three independent trials. Red circles, k_1, $m_f^{\ddagger}$=0.3 kcal/mol; orange triangles, k_2, $m_f^{\ddagger}$=0.4 kcal/mol; green squares, k_3, $m_f^{\ddagger}$=0.6-kcal/mol, $m_u^{\ddagger}$=−0.6 kcal/mol; blue diamonds, k_4, $m_f^{\ddagger}$=0.6-kcal/mol. The data were fit to $k_{obs} \approx k_f = \exp(b_f + m_f^{\ddagger}\ \ln C)$ or $k_3 \approx k_f + k_u = \exp(b_f + m_f^{\ddagger}\ \ln C) + \exp(b_u + m_u^{\ddagger}\ \ln C)$, which assumes a linear change in $\Delta G^{\ddagger}$ with ln*C*.

If, like the folding free energy, the transition-state free energy $\Delta G^{\ddagger}$ is assumed to vary linearly with lnC,[29] then the forward or reverse rate constant for each step can be expressed as $\ln k = \ln k_o - \Delta G^{\ddagger}/RT = \ln k_o - \Delta G^{\ddagger}_{ref}/RT + m^{\ddagger}\ln C$, in which k_o is the folding rate when $\Delta G^{\ddagger} = 0$ and $\Delta G^{\ddagger}_{ref}$ is the transition-state free energy in 1 mM $MgCl_2$. This simple model fit the kinetic data well, within the error of the observed rate constants (Fig. 6). The dependence of $\Delta G^{\ddagger}$ on Mg^{2+} (lnC) ranged from 0.3 to 0.6 kcal/mol at 37 °C for the various rate constants, about half the magnitude of −1.0 kcal/mol for the equilibrium between I_C and N (Fig. 3b). This suggests that the transition-state ensembles are less structured than the native state.

Fast Fenton footprinting reveals reorganization of the ribozyme core

The stopped-flow fluorescence data show that about 45% of the fluorescent signal associated with folding occurs slowly, over 10 s. On the other hand, previous time-resolved hydroxyl radical footprinting showed that tertiary interactions throughout the wild-type ribozyme formed in 5–20 ms.[10] Therefore, the slow changes in 2-AP fluorescence might represent conformational steps that are not detected by hydroxyl radical footprinting. Alternatively, the slow decrease in 2-AP fluorescence might reflect new intermediates caused by the nick in the P9 tetraloop, which is critical for the stability of the ribozyme core.[30] To distinguish between these possibilities and assign the fluorescent signals to specific structural changes in the RNA, we carried out time-resolved footprinting on the IΔP9–OP9 complex under conditions as similar as possible to those used for the stopped-flow fluorescence experiments (Fig. S5).

The IΔP9–OP9G complex was preformed in 0.5 mM $MgCl_2$ and then rapidly mixed with $MgCl_2$ (15 mM final) at 37 °C to begin the folding reaction. The tertiary structure of the RNA was probed using the fast Fenton reaction method, which resolves conformational changes within 5 ms.[31] Unlike the unimolecular ribozyme, the backbone of the IΔP9–OP9G complex was protected in two or three stages, indicating the presence of tertiary folding intermediates (Fig. 7; Table S1). Since the protection patterns of the fully folded IΔP9–OP9G and unimolecular ribozymes match closely, the change in the observed folding rates had to come from a change in the folding pathway of the IΔP9–OP9G ribozyme.

First, we observed that all of the expected segments of the IΔP9–OP9G backbone were rapidly protected from hydroxyl radical cleavage, with transition midpoints shorter than 5 ms ($k_{obs} \geq 100\ s^{-1}$) (Fig. 7a and b). On average, the backbone protections were

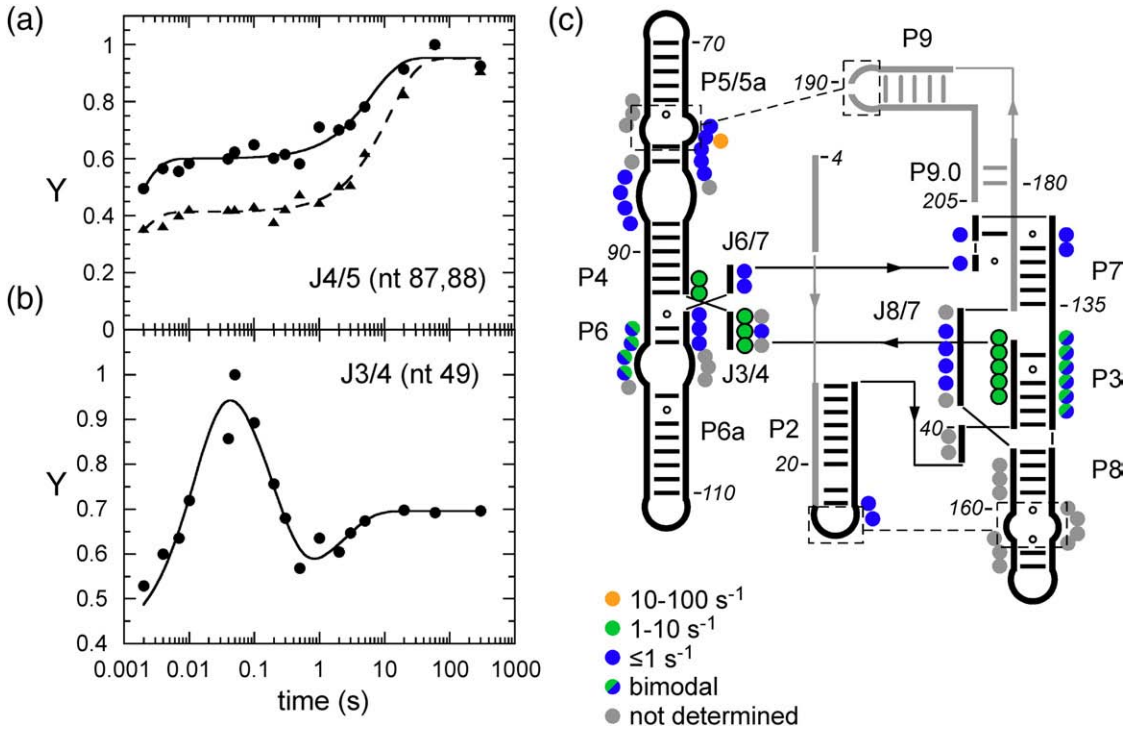

Fig. 7. Tertiary folding kinetics of nicked ribozyme by hydroxyl radical footprinting. Folding kinetics of IΔP9·OP9G ribozyme at 37 °C in 15 mM $MgCl_2$ were measured by time-resolved footprinting (see Materials and Methods). (a) Relative saturation of backbone protection (*Y*) versus folding time for nucleotide 87 (triangles) and nucleotide 88 (circles). Data were scaled to the unfolded and fully folded RNA and fit to a biexponential rate equation (see Materials and Methods). (b) Saturation of nucleotide 49 as in (a); arbitrary *Y* scale shows fluctuations in the relative cleavage of these residues over time. (c) Residues participating in slow refolding steps are colored as in the key. All of these residues except nucleotide 62 are also 40–60% protected in the first 10 ms ($k_1 \geq 100\ s^{-1}$). Regions that could not be reliably analyzed are shown in gray in the schematics.

40–60% saturated relative to the native state within this initial period, consistent with the fraction of rapidly folding RNA obtained from fluorescence studies. Thus, the tertiary interactions form rapidly in the 2-AP-labeled ribozyme but to a lesser extent than in the unimolecular ribozyme.

The rate of backbone protection was slightly faster than the apparent folding rate monitored by fluorescence ($k_2 = 34\ s^{-1}$). Fluorescence emission reports the microenvironment of 2-AP at position 191, and its slower rate of change may reflect weaker docking of the nicked P9 tetraloop with its receptor. The P5/5a receptor for the P9 tetraloop (nucleotide 62) was protected more slowly ($20\ s^{-1}$) than adjacent residues and to a smaller degree (25–30%). Thus, the footprinting results support the interpretation that the docked P9 complex is less stable or more dynamic than expected.

Second, we used the footprinting data to obtain a more detailed explanation for the slow steps of folding, which account for about half of the dynamic change in the RNA (Fig. 7c). In the ribozyme core, the slow rate constants for protection of P4, P6, J6/6a, and P3 overlapped with each other, in the range of 0.15–0.5 s^{-1}. Residues involved in other tertiary interactions saturated even more slowly (0.02–0.08 s^{-1}). The similarity between these values and the slowest phase of fluorescence emission decay (k_4), which accounts for 40–45% of the population, strongly supports the assumption that this step arises from reorganization of the RNA tertiary (and secondary) structure. We cannot judge, however, whether this reorganization is a concerted motion throughout the ribozyme core or a series of local movements with slightly different rate constants, for which fluorescence can only report an average rate.

Unlike residues elsewhere in the structure, the slow rate constants for the protection of J6/6a (nucleotides 95–99) and P3 (nucleotides 137–141) could not be precisely determined. Instead, probable solutions to the rate equations covered the range of 0.5–5 s^{-1}. As these two regions interact in an A-minor motif in the native ribozyme,[17] it is unlikely that this indetermination is simply a result of random noise in the data. Rather, this spread in the probable values of the rate constants may be due to averaging of two underlying processes with different rates. We speculate that P3 and J6/6a, or the pseudoknot belt that partially covers P3 and P6, undergo a structural change at a rate of 1–5 s^{-1} that is responsible for the fluorescence decrease at 1 s^{-1} (k_3). These residues are additionally protected by the slow reorganization of folding intermediates at 0.1 s^{-1} (k_4), either subsequent to the preceding step or in parallel with it.

This model is further supported by direct evidence for refolding of the P3 pseudoknot from the time-resolved footprinting data (Fig. 7c). The pseudoknot "belt" (nucleotides 39–54) is normally exposed to solvent in the native ribozyme,[9] except for nucleotides 49–50 that form part of the central triple helix (J3/4). In our experiments, however, nucleotides 43–52 were rapidly protected from cleavage ($k \geq 100\ s^{-1}$) and then exposed with an average rate constant of $5.4 \pm 0.8\ s^{-1}$ (Table S2). Therefore, the decay rate of 1 s^{-1} in the fluorescence data most likely captures refolding of misfolded intermediates lacking the P3 pseudoknot. Residues 49–50 showed the same behavior, but the extent of protection slowly increased again after 1 s with a rate constant of $k \sim 0.3\ s^{-1}$ (Fig. 7b). In the fully folded RNA, nucleotides 49–50 are protected from hydroxyl radical cleavage as expected.

Discussion

The concordance of multiple structural probes can reveal new features of RNA folding pathways (e.g., Refs. [32,33]). In our study, a side-by-side comparison of stopped-flow fluorescence and time-resolved footprinting measurements allowed the collective behavior of individual residues to be correlated with global steps in the folding pathway. Stringent statistical analysis of the rate constants revealed steps in the refolding pathway that were not initially obvious. In addition, the shorter dead time of the stopped-flow spectrometer (1.8 ms *versus* 5 ms for footprinting) demonstrated that the earliest folding transitions of the *Azoarcus* ribozyme occur in ≤10 ms at 37 °C.

As expected from previous work,[9] the 2-AP-labeled ribozyme exhibited two distinct equilibrium folding transitions as a function of Mg^{2+} concentration. The first transition appeared at the same Mg^{2+} concentration as the $U \rightarrow I_C$ collapse transition monitored by SAXS and other methods.[11] By contrast, the Mg^{2+} requirement for the second transition is in good agreement with the midpoint of the $I_C \rightarrow N$ tertiary folding transition monitored using biochemical probes. That the fluorescence transitions in the P3 mutant ribozyme occurred at higher magnesium concentrations further supports the conclusion that the change in fluorescence emission represents global folding transitions rather than local perturbations to the probe environment. Additional folding transitions may overlap these two main phase transitions, such as a non-sequence-specific contraction of the RNA in low Mg^{2+}. Similarly, catalytic activity increases more cooperatively with respect to Mg^{2+} than backbone accessibility or fluorescence. Thus, formation of the native RNA may involve two overlapping transitions leading to a folded, inactive RNA (I_F) and to the active ribozyme (N).[34]

The folding kinetics of the 2-AP-labeled *Azoarcus* ribozyme were unexpectedly complex, with at least four time-dependent transitions (Fig. 8). The multistage folding kinetics observed by stopped-flow fluorescence can be explained either by partitioning of the population among parallel folding pathways with different transition states or by sequential changes in the structure of the RNA, each producing a change in the environment of the fluorophore. However, the immediate partial saturation of backbone contacts everywhere in the RNA is most easily explained if part of the RNA population folds very rapidly. Thus, the results of the footprinting experi-

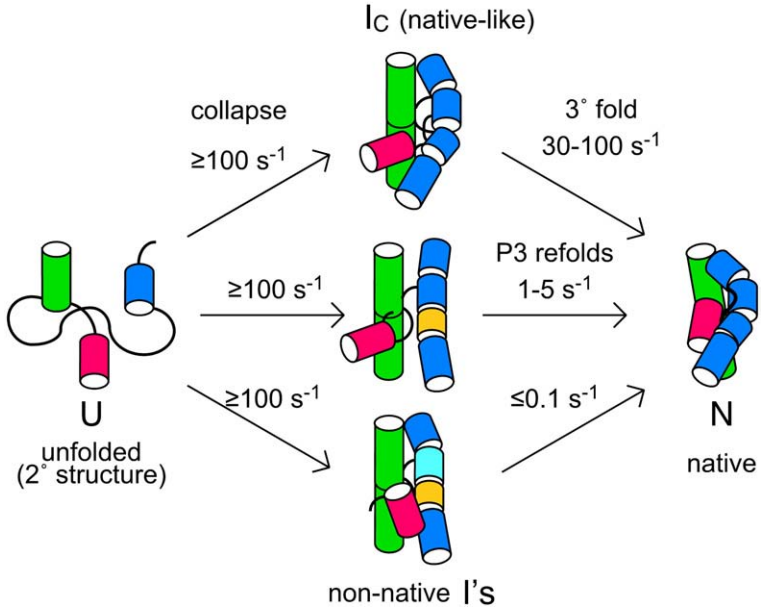

Fig. 8. Model of ribozyme folding pathways. Based on the data presented here and elsewhere,[9–12] the initial ensemble of secondary structures (U) collapses into native-like (I_C) and nonnative intermediates (I's) when the concentration of Mg^{2+} is raised above 0.3 mM. In 15 mM $MgCl_2$ at 37 °C, native-like intermediates form the native tertiary structure at $\geq 100\ s^{-1}$. In the nicked IΔP9·OP9G ribozyme, nonnative intermediates with P3 mispaired (gold cylinder) require reorganization of the ribozyme core (1 and 0.1 s^{-1}). For simplicity, we assume that these slow steps occur in parallel, but the data could also be explained by sequential refolding events along the slow pathway.

ments are most consistent with partitioning among fast and slow folding pathways (Fig. 8).

In our model, we propose that both collapse and the initial formation of tertiary interactions occur within 10 ms in 15 mM $MgCl_2$. These steps are not well resolved in our experiments, especially as the folding trajectories begin with a mixture of U and I_C in 0.5 mM $MgCl_2$. For about half the IΔP9·OP9G ribozyme population, these transitions lead directly to the native tertiary structure. Partial protection of the 5′ side of P3 (nucleotides 43–52), which is exposed to solvent in the native ribozyme, suggests that nonnative intermediates are also formed within this time. Both the fluorescence and footprinting results suggest that in the IΔP9·OP9G complex, docking of P9 lags behind tertiary interactions in the rest of the RNA (34 s^{-1}). This fluorescence signal may alternatively represent a local conformational change in the P9 tetraloop, but the activation energy of this step (35 kcal/mol·K) is more consistent with a larger structural rearrangement.

Next, we propose that the slow folding steps arise from RNA molecules that initially fail to form the P3 pseudoknot during the collapse transition. The P3 pseudoknot is universally conserved among group I ribozymes and required for ribozyme activity.[35] Mispairing of P3 causes the *Tetrahymena* ribozyme to become kinetically trapped in metastable folding intermediates *in vitro*,[36] and such a possibility for the *Azoarcus* ribozyme was suggested by previous ribonuclease probing studies on the pre-tRNA and predicted secondary structures.[37,38]

The misfolded intermediates of the *Azoarcus* ribozyme are resolved in at least two steps: refolding of the interface between P3, P4, and P6 at 1–5 s^{-1}, which exposes residues in P3, and the formation of core tertiary interactions at ~0.1 s^{-1} or slower. The burial, exposure, and reburial of residues in J3/4 may be explained by either sequential or parallel folding routes, although for the reasons given above, we favor a parallel model (Fig. 8). The slowest kinetic step may include a rearrangement of the G-binding pocket in the active site, similar to that reported for the *Tetrahymena* ribozyme.[39,40]

In conclusion, the *in vitro* refolding rates of ribozymes vary dramatically, with some sequences achieving their native structure within 10 ms and others requiring 100 s or longer.[4,5] This variation in folding times can be explained by the kinetic partitioning of RNA populations among native-like and nonnative folding intermediates, as the latter require long times to refold. The combination of fluorescence and hydroxyl radical footprinting corroborates our previous findings that the tertiary structure of the *Azoarcus* ribozyme forms rapidly (~10 ms) in 10–15 mM $MgCl_2$ once the secondary structure of the RNA has been established.[9,10] The *Azoarcus* ribozyme is unusually stable,[8] and this may explain why a large fraction of the population appears to fold directly to the native state.

We previously found that single base substitutions in the P9 tetraloop that destabilize the ribozyme's tertiary structure also lowered the fraction of fast-folding RNA, by diverting a larger portion of the population through metastable folding intermediates.[10] Here, we observe that a nick in P9 has a similar effect on the proportions of native-like and nonnative folding intermediates. In both cases,

perturbations to P9 affect folding of the entire RNA, consistent with the importance of these interactions in group I introns.[41] That even small perturbations to the tertiary structure increase the heterogeneity of the folding dynamics illustrates the tight connection between the thermodynamic stability of the tertiary interactions and the accuracy of the folding process.[10] This correlation has important consequences for the evolution of RNA sequences and for the assembly of large ribonucleoprotein complexes.

Materials and Methods

Plasmids and RNA preparation

Plasmids encoding (L-3) IΔP9 ribozyme with wild-type core or containing the P3 mutation G44C were prepared by PCR amplification of pAz-IVS and pAzG44CIVS, respectively, using the downstream primer 5′ CGC CTG CAG AAA CTC TTC ATC GCC ACT CCC TGG ACT AT 3′ and the upstream primer 5′CGC GAA TTC TAA TAC GAC TCA CTA TAG GCG ATG TGC CTT GCG CCG GGA 3′. The primers contain EcoRI and PstI restriction site insertion into pUC18.

The (L-3) IΔP9 ribozyme was transcribed *in vitro* with T7 RNA polymerase from plasmid DNA digested to completion with EarI. Transcription reactions (10 mL) were carried out in disposable 50-mL centrifuge tubes and purified by denaturing 4% (w/v) PAGE as described earlier.[12] The eluate was pooled and exchanged 4 times with 10 mM Tris–HCl (pH7.5) using Centricon Plus-30 concentrators (Amicon) at 4 °C. The concentration of (L-3) IΔP9 RNA was determined using absorption at 260 nm (extinction coefficient of 1.82×10^6 L/mol·cm).

Preparation of fluorescently labeled oligonucleotides

The OP9G fluorescent oligonucleotide [5′ r(2-AP) AGC CAC ACA AAC CG 3′] was obtained from Dharmacon (Boulder, CO). OP9G anneals to the 3′ end of the IΔP9 ribozyme fragment so that 2-AP replaces A191. U194 was replaced with C to increase the stability of the complex.[17] The oligonucleotide was deprotected and purified on a denaturing 15% polyacrylamide gel following the manufacturer's protocols. The purified RNA was resuspended in 10 mM Tris–HCl (pH7.5), and the concentration was estimated using $\varepsilon_{260}=1.39\times10^5$ L/mol·cm.

Oligonucleotide gel-shift experiments

OP9G oligonucleotide was 5′-labeled with ^{32}P and gel purified using standard methods. Radiolabeled oligomer (15 nM) was annealed with 0–20 μM (L-3) IΔP9 RNA in 10 mM Tris–HCl (pH7.5), in 10 μl reaction volume, for 2 min at 65 °C followed by 1 min on ice. Samples (2 μl) were loaded on a 10% (w/v) native polyacrylamide gel [29:1 acrylamide/bis, 34 mM Tris, 66 mM Hepes, 0.1 mM ethylenediaminetetraacetic acid (EDTA), and 0.5 mM $MgCl_2$] at 4 °C and electrophoresed at 15 W for 1.5 h. Dried gels were quantified using a Molecular Dynamics PhosphorImager. The fraction of oligomer bound to (L-3) IΔP9 RNA, f_B, was determined from the counts in the shifted bands (B) relative to the total counts (B+F) in the lane and normalized to the extent of binding at saturation. The binding data were fit to a single-site binding isotherm to obtain the equilibrium dissociation constant.

Self-cleavage activity

DNA templates for T7 runoff transcription of RNAs starting 33 nt upstream of the 5′ splice site and ending in G205 (5′ ex-I) or A190 (5′ ex-IΔP9) were constructed by PCR. Self-splicing reactions were carried out in 25 mM Na–Hepes as previously described.[8] For reactions with IΔP9, 20 nM uniformly labeled RNA was annealed to 0.5 μM OP9. Reactions were initiated with GTP (100 μM) and stopped with 30 mM EDTA.

Equilibrium fluorescence measurements

Steady-state fluorescence experiments were carried out on an Aviv ATF105 spectrofluorometer in a 500-μl quartz cuvette with 1 cm path length (Hellma Biotech). All equilibrium experiments were carried out in 10 mM Tris–HCl (pH7.5) buffer. The fluorescently tagged *Azoarcus* RNA for the equilibrium measurements was prepared by annealing 2 μM OP9G oligonucleotide with 10 μM (L-3) IΔP9 RNA in 10 mM Tris–HCl (pH7.5) at 65 °C for 1 min, followed by slow cooling to room temperature. A 5-fold excess of (L-3) IΔP9 RNA was used to ensure that all the 2-AP oligonucleotide was bound.

The annealed RNA was transferred to the cuvette for fluorescence measurements where the $MgCl_2$ was incrementally increased from 0 to 15 mM. The sample was incubated at 37 °C for 5 min after each addition before taking the reading. The 2-AP excitation wavelength was set to 310 nm and the emission spectra were collected from 325 to 425 nm using 5 mm excitation and emission slit widths. The fluorescence intensity was recorded at the emission maximum of 2-AP (370 nm) and corrected for the small dilution caused by the titrant.

The emission intensity as a function of Mg^{2+} concentration, F(Mg), was normalized using $F=[F(\mathrm{Mg})-F_{\min}]/[F_{\max}-F_{\min}]$, in which $F_{\min}$ and $F_{\max}$ represent the minimum and maximum fluorescence signals over the Mg^{2+} titration. The relative fluorescence F was fit to a three-state model, $F=\chi_U F_U+\chi_I F_I+\chi_N F_N$, in which F_U, F_I, and F_N are the fluorescence intensities of the U, I_C, and N, respectively, and χ_i's are the mole fraction of each species. For the wild-type RNA, $F_U=0.6$, $F_I=1$, and $F_N=0$. For the P3 mutant RNA, $F_U=0$, $F_I=1$, and $F_N=0.3$. The mole fraction of each species was obtained from fits to Eq. (1).

$$F=\frac{[F_U+F_I(C/C_I)^m+F_N(C/C_N)^n]}{[1+(C/C_I)^m+(C/C_N)^n]} \quad (1)$$

The statistical weights of each term represent the free-energy difference between the U and I_C or U and N states and are assumed to take the form $\Delta G=-RT(n\ln C-n\ln C_N)$, in which C is the Mg^{2+} concentration, C_I or C_N is the midpoint of each transition, and m and n represent the cooperativity of each transition with respect to Mg^{2+} concentration.[21,29] Because the two transitions are well separated, the data were fit equally well by sequential two-state transitions (U to I_C and I_C to N), although this model slightly overestimates the concentration of I_C.

Stopped-flow kinetic measurements

Time-dependent refolding experiments were carried out on an Applied Photophysics stopped-flow spectrofluo-

rometer (SX.18MV) with a mixing dead time of 1.8 ms. The 2-AP-tagged ribozyme was prepared by annealing 4 μM U194C-OP9G with 20 μM (L-3) IΔP9 RNA in 10 mM Tris–HCl plus 0.5 mM Mg^{2+} at 65 °C for 5 min, followed by slow cooling to room temperature. The addition of 0.5 mM Mg^{2+} significantly increased the affinity of OP9G oligonucleotide for (L-3) IΔP9 RNA. In addition, a 5-fold excess of (L-3) IΔP9 RNA was used to ensure that all the 2-AP oligonucleotide was bound. Folding reactions were initiated by mixing equal volumes (100 μl) of RNA solution and buffered $MgCl_2$ (0–15 mM final). Solutions were pre-equilibrated 10 min at 37 °C before mixing.

Excitation was at 310 nm, and the change in fluorescence emission was measured using a wide band cutoff filter of 360 nm. At least six time traces with 1000 points per window were collected for each data set. The raw fluorescence intensities were normalized to the minimum and maximum signal observed during the course of each folding trajectory. The relative change in fluorescence recorded over 10 s and 500 ms was fit to $F = A_0 + A_1(1 - e^{-k_1 t}) + A_2(1 - e^{-k_2 t})$ and $F = A_0 + A_1(1 - e^{-k_1 t}) + A_2(1 - e^{-k_2 t}) + A_3(1 - e^{-k_3 t})$, respectively. The observed rate constants for six traces were averaged. Data collected over 500 ms were used to measure the first two kinetic phases; data collected over 10 s provide better resolution of the last two kinetic phases. We could not accurately determine the amplitudes of the phases observed in different collection time windows. For certain conditions, data sets were concatenated by scaling the 500-ms data to the relative fluorescence at $t = 500$ ms in the 10-s data set. The amplitudes were estimated from multiphasic fits to the combined data to 10 s.

Time-resolved footprinting

(L-3) IΔP9 RNA (40 pmol) was 5′-end-labeled with [^{32}P] ATP and gel purified according to standard methods. IΔP9 RNA (50 nM) was annealed with 2 μM OP9G in 10 mM Na-cacodylate and 1 mM EDTA (CE) plus 0.5 mM $MgCl_2$ for 1 min at 65 °C and then placed on ice. For control reactions on completely folded RNA, $MgCl_2$ was added to 15 mM (final) and incubated for 20 min at 50 °C. Time-resolved hydroxyl radical footprinting reactions were carried out with the Fenton reaction as previously described,[10,42] except that the control software and protocols were slightly modified to optimize the RNA recovery.

The cleavage products in sequencing gels were quantified using SAFA (nucleotides 24 to 104)[43] or IMAGEQUANT (Molecular Dynamics). Five invariable products (residues 25, 64, 73, 74, and 102) were used to standardize the band intensities.[44] The extent and rates of protections were determined by normalizing relative saturation of each protection Y to the unfolded and folded controls (0 to 1, respectively) and fitting to first-order rate equations as above. In parts of the sequence where high noise levels prevented the use of folded and unfolded controls for normalization, protections were scaled between maximum and minimum intensities.

Statistical analysis of parameters

Each transition was subjected to a bootstrap analysis[45] with 5000 resampling of fit residuals performed within MATLAB (Mathworks, Natick, MA) to assess the reliability of kinetics parameters obtained from footprinting experiments. Outlier values were detected and removed by the method of Hoaglin *et al.*[46] with boundaries set at 1.5 interquartile region distances from first and third quartiles. The resultant distributions were used to obtain a symmetric region around most probable value (mode) encompassing 95% of observations. When the noise in the data resulted in more than one significant peak in the parameter distribution (e.g., residues 137–141), the corresponding fits were treated independently to obtain different but equally probable sets of amplitudes and rate constants.

Acknowledgements

The authors thank D. Draper and M. Brenowitz for their assistance and advice. This work was supported by a grant from the National Institutes of Health (GM60819).

Supplementary Data

Supplementary data associated with this article can be found, in the online version, at doi:10.1016/j.jmb.2008.12.075

References

1. Lilley, D. M. (2005). Structure, folding and mechanisms of ribozymes. *Curr. Opin. Struct. Biol.* **15**, 313–323.
2. Serganov, A. & Patel, D. J. (2007). Ribozymes, riboswitches and beyond: regulation of gene expression without proteins. *Nat. Rev. Genet.* **8**, 776–790.
3. Winkler, W. C. & Breaker, R. R. (2005). Regulation of bacterial gene expression by riboswitches. *Annu. Rev. Microbiol.* **59**, 487–517.
4. Thirumalai, D. & Hyeon, C. (2005). RNA and protein folding: common themes and variations. *Biochemistry*, **44**, 4957–4970.
5. Sosnick, T. R. & Pan, T. (2003). RNA folding: models and perspectives. *Curr. Opin. Struct. Biol.* **13**, 309–316.
6. Al-Hashimi, H. M. & Walter, N. G. (2008). RNA dynamics: it is about time. *Curr. Opin. Struct. Biol.* **18**, 321–329.
7. Thirumalai, D., Lee, N., Woodson, S. A. & Klimov, D. (2001). Early events in RNA folding. *Annu. Rev. Phys. Chem.* **52**, 751–762.
8. Tanner, M. & Cech, T. (1996). Activity and thermostability of the small self-splicing group I intron in the pre-tRNA(lle) of the purple bacterium *Azoarcus*. *RNA*, **2**, 74–83.
9. Rangan, P., Masquida, B., Westhof, E. & Woodson, S. A. (2003). Assembly of core helices and rapid tertiary folding of a small bacterial group I ribozyme. *Proc. Natl Acad. Sci. USA*, **100**, 1574–1579.
10. Chauhan, S. & Woodson, S. A. (2008). Tertiary interactions determine the accuracy of RNA folding. *J. Am. Chem. Soc.* **130**, 1296–1303.
11. Perez-Salas, U. A., Rangan, P., Krueger, S., Briber, R. M., Thirumalai, D. & Woodson, S. A. (2004). Compaction of a bacterial group I ribozyme coincides with the assembly of core helices. *Biochemistry*, **43**, 1746–1753.
12. Chauhan, S., Caliskan, G., Briber, R. M., Perez-Salas, U., Rangan, P., Thirumalai, D. & Woodson, S. A. (2005).

RNA tertiary interactions mediate native collapse of a bacterial group I ribozyme. *J. Mol. Biol.* **353**, 1199–1209.
13. Ward, D. C., Reich, E. & Stryer, L. (1969). Fluorescence studies of nucleotides and polynucleotides. I. Formycin, 2-aminopurine riboside, 2,6-diaminopurine riboside, and their derivatives. *J. Biol. Chem.* **244**, 1228–1237.
14. Millar, D. P. (1996). Fluorescence studies of DNA and RNA structure and dynamics. *Curr. Opin. Struct. Biol.* **6**, 322–326.
15. Jean, J. M. & Hall, K. B. (2001). 2-Aminopurine fluorescence quenching and lifetimes: role of base stacking. *Proc. Natl Acad. Sci. USA*, **98**, 37–41.
16. Ikawa, Y., Naito, D., Aono, N., Shiraishi, H. & Inoue, T. (1999). A conserved motif in group IC3 introns is a new class of GNRA receptor. *Nucleic Acids Res.* **27**, 1859–1865.
17. Adams, P. L., Stahley, M. R., Kosek, A. B., Wang, J. & Strobel, S. A. (2004). Crystal structure of a self-splicing group I intron with both exons. *Nature*, **430**, 45–50.
18. Juneau, K., Podell, E., Harrington, D. J. & Cech, T. R. (2001). Structural basis of the enhanced stability of a mutant ribozyme domain and a detailed view of RNA–solvent interactions. *Structure*, **9**, 221–231.
19. Cate, J. H., Gooding, A. R., Podell, E., Zhou, K., Golden, B. L., Kundrot, C. E. *et al.* (1996). Crystal structure of a group I ribozyme domain: principles of RNA packing. *Science*, **273**, 1678–1685.
20. Abramovitz, D. L. & Pyle, A. M. (1997). Remarkable morphological variability of a common RNA folding motif: the GNRA tetraloop–receptor interaction. *J. Mol. Biol.* **266**, 493–506.
21. Fang, X., Pan, T. & Sosnick, T. R. (1999). A thermodynamic framework and cooperativity in the tertiary folding of a Mg(2+)-dependent ribozyme. *Biochemistry*, **38**, 16840–16846.
22. Emerick, V. L. & Woodson, S. A. (1993). Self-splicing of the *Tetrahymena* pre-rRNA is decreased by misfolding during transcription. *Biochemistry*, **32**, 14062–14067.
23. Rook, M. S., Treiber, D. K. & Williamson, J. R. (1998). Fast folding mutants of the *Tetrahymena* group I ribozyme reveal a rugged folding energy landscape. *J. Mol. Biol.* **281**, 609–620.
24. Russell, R. & Herschlag, D. (1999). New pathways in folding of the *Tetrahymena* group I RNA enzyme. *J. Mol. Biol.* **291**, 1155–1167.
25. Gluick, T. C., Gerstner, R. B. & Draper, D. E. (1997). Effects of Mg^{2+}, K^{+}, and H^{+} on an equilibrium between alternative conformations of an RNA pseudoknot. *J. Mol. Biol.* **270**, 451–463.
26. Li, Y., Bevilacqua, P. C., Mathews, D. & Turner, D. H. (1995). Thermodynamic and activation parameters for binding of a pyrene-labeled substrate by the *Tetrahymena* ribozyme: docking is not diffusion-controlled and is driven by a favorable entropy change. *Biochemistry*, **34**, 14394–14399.
27. Matthews, C. R. (1987). Effect of point mutations on the folding of globular proteins. *Methods Enzymol.* **154**, 498–511.
28. Kiefhaber, T. (1995). Protein folding kinetics. *Methods Mol. Biol.* **40**, 313–341.
29. Pan, J., Thirumalai, D. & Woodson, S. A. (1999). Magnesium-dependent folding of self-splicing RNA: exploring the link between cooperativity, thermodynamics, and kinetics. *Proc. Natl Acad. Sci. USA*, **96**, 6149–6154.
30. Jaeger, L., Michel, F. & Westhof, E. (1994). Involvement of a GNRA tetraloop in long-range RNA tertiary interactions. *J. Mol. Biol.* **236**, 1271–1276.
31. Shcherbakova, I., Mitra, S., Beer, R. H. & Brenowitz, M. (2006). Fast Fenton footprinting: a laboratory-based method for the time-resolved analysis of DNA, RNA and proteins. *Nucleic Acids Res.* **34**, e48.
32. Russell, R., Zhuang, X., Babcock, H. P., Millett, I. S., Doniach, S., Chu, S. & Herschlag, D. (2002). Exploring the folding landscape of a structured RNA. *Proc. Natl Acad. Sci. USA*, **99**, 155–160.
33. Kwok, L. W., Shcherbakova, I., Lamb, J. S., Park, H. Y., Andresen, K., Smith, H. *et al.* (2006). Concordant exploration of the kinetics of RNA folding from global and local perspectives. *J. Mol. Biol.* **355**, 282–293.
34. Rangan, P. & Woodson, S. A. (2003). Structural requirement for Mg^{2+} binding in the group I intron core. *J. Mol. Biol.* **329**, 229–238.
35. Michel, F. & Westhof, E. (1990). Modelling of the three-dimensional architecture of group I catalytic introns based on comparative sequence analysis. *J. Mol. Biol.* **216**, 585–610.
36. Pan, J. & Woodson, S. A. (1998). Folding intermediates of a self-splicing RNA: mispairing of the catalytic core. *J. Mol. Biol.* **280**, 597–609.
37. Rangan, P., Masquida, B., Westhof, E. & Woodson, S. A. (2004). Architecture and folding mechanism of the *Azoarcus* Group I Pre-tRNA. *J. Mol. Biol.* **339**, 41–51.
38. Zhang, L., Xiao, M., Lu, C. & Zhang, Y. (2005). Fast formation of the P3-P7 pseudoknot: a strategy for efficient folding of the catalytically active ribozyme. *RNA*, **11**, 59–69.
39. Zarrinkar, P. P. & Sullenger, B. A. (1998). Probing the interplay between the two steps of group I intron splicing: competition of exogenous guanosine with omega G. *Biochemistry*, **37**, 18056–18063.
40. Karbstein, K. & Herschlag, D. (2003). Extraordinarily slow binding of guanosine to the *Tetrahymena* group I ribozyme: implications for RNA preorganization and function. *Proc. Natl Acad. Sci. USA*, **100**, 2300–2305.
41. Jaeger, L., Westhof, E. & Michel, F. (1993). Monitoring of the cooperative unfolding of the sunY group I intron of bacteriophage T4. The active form of the sunY ribozyme is stabilized by multiple interactions with 3′ terminal intron components. *J. Mol. Biol.* **234**, 331–346.
42. Shcherbakova, I., Mitra, S., Beer, R. H. & Brenowitz, M. (2008). Following molecular transitions with single residue spatial and millisecond time resolution. *Methods Cell Biol.* **84**, 589–615.
43. Das, R., Laederach, A., Pearlman, S. M., Herschlag, D. & Altman, R. B. (2005). SAFA: semi-automated footprinting analysis software for high-throughput quantification of nucleic acid footprinting experiments. *RNA*, **11**, 344–354.
44. Takamoto, K., Chance, M. R. & Brenowitz, M. (2004). Semi-automated, single-band peak-fitting analysis of hydroxyl radical nucleic acid footprint autoradiograms for the quantitative analysis of transitions. *Nucleic Acids Res.* **32**, E119.
45. Efron, B. & Tibshirani, R. J. (1993). An introduction to the bootstrap. *Monographs on Statistics and Applied Probability*, vol. 57, pp. Chapman & Hall, New York, NY.
46. Tukey, J. W. (1977). *Exploratory Data Analysis*, Addison-Wesley Publishing Company, Reading, MA.